ORIGINAL PAPER



Effect of pH on the activity of ice-binding protein from *Marinomonas* primoryensis

Elizabeth A. Delesky¹ · Patrick E. Thomas^{2,3} · Marimikel Charrier⁴ · Jeffrey C. Cameron^{2,3,5} · Wil V. Srubar III^{1,4} D

Received: 19 June 2020 / Accepted: 29 September 2020 / Published online: 22 October 2020 © Springer Japan KK, part of Springer Nature 2020

Abstract

The ability of an ice-binding protein (IBP) from *Marinomonas primoryensis* (MpIBP) to influence ice crystal growth and structure in nonphysiological pH environments was investigated in this work. The ability for MpIBP to retain ice interactivity under stressed environmental conditions was determined via (1) a modified splat assay to determine ice recrystallization inhibition (IRI) of polycrystalline ice and (2) nanoliter osmometry to evaluate the ability of MpIBP to dynamically shape the morphology of a single ice crystal. Circular dichroism (CD) was used to relate the IRI and DIS activity of MpIBP to secondary structure. The results illustrate that MpIBP secondary structure was stable between pH 6 and pH 10. It was found that MpIBP did not interact with ice at $pH \le 4$ or $pH \ge 13$. At $6 \le pH \ge 12$ MpIBP exhibited a reduction in grain size of ice crystals as compared to control solutions and demonstrated dynamic ice shaping at $6 \le pH \ge 10$. The results substantiate that MpIBP retains some secondary structure and function in non-neutral pH environments; thereby, enabling its potential utility in nonphysiological materials science and engineering applications.

Keywords Ice-binding proteins · Antifreeze proteins · pH · Ice recrystallization inhibition · Dynamic ice shaping

Introduction

Previous research indicates that ice-binding proteins (IBPs) may offer an alternative to conventional frost–prevention strategies for biological cryopreservation (Davies 2014; Liang et al. 2016) and, by extension, antifreeze applications in a host of other commercial industries such as coolants in aerospace engineering, frost–resistant pavements in civil

Communicated by A. Driessen.

Electronic supplementary material The online version of this article (https://doi.org/10.1007/s00792-020-01206-9) contains supplementary material, which is available to authorized users.

 Wil V. Srubar III wsrubar@colorado.edu

Elizabeth A. Delesky elizabeth.delesky@colorado.edu

Patrick E. Thomas patrick.thomas@colorado.edu

Marimikel Charrier mmcharrier@colorado.edu

Jeffrey C. Cameron jeffrey.c.cameron@colorado.edu

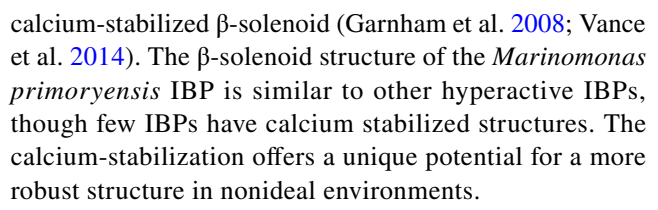
engineering, and anti-icing coatings for energy infrastructure such as solar panels or wind turbines. While IBPs offer a promising biological solution for these ice-growth prevention applications, proteins are well known to unfold, refold, denature, aggregate, or degrade in nonphysiological environments (Ptitsyn 1987). Applications with harsh chemical environments, such as concrete in civil engineering that has a pore solution pH of 12–13 (Ghods et al. 2009), would benefit from a material that inhibits ice recrystallization. Freeze—thaw damage in concrete is due, in part, to the expansion of ice crystals (Powers 1975) demonstrating a need for materials that inhibit ice growth in extreme pH environments. To the authors' knowledge, some studies have

- Materials Science and Engineering Program, University of Colorado Boulder, Boulder, CO 80309, USA
- Department of Biochemistry, University of Colorado Boulder, Boulder, CO 80303, USA
- Renewable and Sustainable Energy Institute, University of Colorado, Boulder, CO 80309, USA
- Department of Civil, Environmental, and Architectural Engineering, University of Colorado Boulder, Boulder, CO 80309, USA
- National Renewable Energy Laboratory, Golden, CO 80401, USA



investigated the effect of pH on thermal hysteresis activity (Chao 1994; Gauthier 1998; Kristiansen and Zachariassen 2005; Li et al. 1998; Wu et al. 1991), and a limited number of studies have indicated that IBPs may produce similar ice recrystallization inhibition (IRI) activity in nonphysiological pH solutions (Leiter et al. 2016; Delesky et al. 2019) which necessitates pH studies for the IRI activity of IBPs in nonphysiological environments.

IBPs are a diverse category of proteins that have evolved independently among many types of organisms, including plants (Duman and Olsen 1993; Griffith et al. 1992; Middleton et al. 2014; Moffatt 2006), fungi (Duman and Olsen 1993; Hoshino et al. 2003; Xiao 2010), fish (Davies 1988; DeVries 1988; Fletcher et al. 1987; Hew et al. 1981; Marshall 2004; Slaughter 1981), insects (Graether et al. 2000; Graham and Davies 2005; Liou et al. 1999), and microbes (Duman and Olsen 1993; Garnham et al. 2008; Gilbert et al. 2004; Vance et al. 2018) to help them survive in freezing environments. As IBPs come from a wide range of organisms, they vary in molecular weight, structure, and activity (Bar-Dolev et al. 2016). X-ray crystallography and NMR studies have resolved IBP structures to include α -helices, β -solenoids, helix bundles, and small globular proteins (Bar-Dolev et al. 2016). Although all structures exhibit the ability to adsorb to ice, there are few trends among residues or sequences that lead to ice binding (Dolev et al. 2016). Mechanistically, the current hypothesis for IBP function is through adsorption-inhibition (Dolev et al. 2016). The ice-binding face of an IBP is composed of regularly spaced ice-binding residues that match the lattice spacing of one or more faces of the ice crystal lattice. The lattice match allows the protein to adsorb to a nascent ice crystal and induce high local curvature on the ice crystal surface that makes further crystal growth energetically unfavorable, a phenomenon known as the Gibbs-Thomson effect (Dolev et al. 2016; Graether et al. 2000; Jia et al. 1996; Knight et al. 1991; Liou et al. 2000). All IBPs exhibit one or more phenomena that indicate their interaction with ice. These phenomena include: (1) thermal hysteresis (TH), a noncolligative depression of freezing point temperature while maintaining (or raising) the melting point; (2) dynamic ice shaping (DIS), a reshaping of the 1H hexagonal ice structure to form less disruptive ice geometries; and (3) ice recrystallization inhibition (IRI), a property that limits ice recrystallization through Ostwald ripening and overall reduces mean crystal size (Voets 2017). Marinomonas primoryensis is an Antarctic bacterium that uses a 1.5 MDa extracellular protein to keep it in the oxygen and nutrient rich phototropic zone by binding to the surface of ice (Dolev et al. 2016). Of the 1.5 MDa protein, a 34 kDa region, dubbed region IV, is responsible for ice binding (Dolev et al. 2016). The ice-binding region consists of mostly β -strands that form a



The purpose of this work was to investigate the ability of the calcium-stabilized ice-binding region IV from the *Marinomonas primoryensis* extracellular adhesion protein (MpIBP) to control the size and inhibit the growth of ice crystals in nonphysiological pH solutions ($2 \le pH \ge 13$). It is not known whether the calcium-stabilized MpIBP is also pH tolerant, thus, we characterized its activity in nonphysiological solutions.

Materials and methods

Materials

All reagents were purchased from Fisher Bioreagents without further purification. Clonal cells with MpIBP were obtained from Dr. Peter Davies at Queen's University in Kingston, Ontario, Canada and used for protein expression (Garnham et al. 2008). Solutions with a pH range from 2 to 13 were created at room temperature in increments of ~ 2 by adding HCl to create acidic solutions and adding NaOH to create basic solutions, and pH was measured again at 0 °C (Table 1). MpIBP at each pH was compared to its respective control pH solution so that all constituents were the same save for the addition of MpIBP. pH 8 was used as the reference solution as it was close to the pH of purification solutions (~8.5). Tris(hydroxymethyl)aminomethane (Tris) was carried over from protein purification and therefore included in control solutions to account for protein addition. Total ionic strength (I) for each solution was calculated according to Eq. (1):

$$I = \frac{1}{2} \sum Z^2 C,\tag{1}$$

where Z is the valence of the ion and C is the concentration. Varied pH solutions were tested for IRI and DIS either as a control or loaded with 0.1 mg/ml MpIBP. A protein concentration of 0.1 mg/ml was used in this study as this was previously determined to be the level at which MpIBP thermal hysteresis activity is at a maximum (Garnham et al. 2008). It was anticipated for MpIBP in pH 4 solution the concentration might have been less than 0.1 mg/ml as pH 4 is close to the isoelectric point of 4.11 (Table S1), which often reduces protein solubility (Xia 2007). The concentration of MpIBP in pH 4 solution was lower than 0.1 mg/ml and measured



Table 1 Solutions for evaluating *Mp*IBP efficacy in different pH conditions

pH			Constituents (mM)					Total ion content			
Target	Ambient	0 °C	Tris	NaCl	CaCl ₂	NaOH	HCl	Na ⁺ (mM)	Cl ⁻ (mM)	I (mol/L)	
2	2.15	3.31	10	15	10	_	32	15	67	0.066	
4	3.99	5.81	10	15	10	_	25	15	60	0.063	
6	6.18	6.93	10	15	10	2.6	26	17.6	61	0.064	
8	8.06	9.21	10	15	10	_	8.5	15	43.5	0.054	
10	9.98	10.52	10	15	10	8.4	2.5	23.4	37.5	0.055	
12	12.01	13.08	10	15	10	44	_	59	35	0.078	
13	12.98	*14+	10	15	10	219	_	234	35	0.207	

^{*}Measured pH was above the threshold of the pH meter

using UV–Vis at 280 nm and was found to be ~ 0.04 mg/ml (Table S2). Table S3 provides the composition for solutions used during MpIBP production and purification procedures.

Expression of MpIBP

Expression of MpIBP was adapted from Garnham et al. (2008). Briefly, a culture was used to inoculate 1.6 L of lysogeny broth (LB) medium with kanamycin (100 µg/mL) and grown until OD₆₀₀ reached 0.5 (37 °C, 200 rpm). The temperature was lowered to 23 °C until cells reached OD₆₀₀ = 1 (~2 h). Then, isopropyl β -D-1-thiogalactopyranoside was added to a final concentration of 1 mM to induce expression overnight. Cells were recovered by centrifugation (30 min, 4300 g, 4 °C), resuspended in Buffer A (Table S2), and lysed using a Qsonica Q55 Sonicator Ultrasonic Homogenizer with Probe 55 W (5x, 45 s, 50% amplitude). Cellular debris was removed via centrifugation (1.5 h, 4 °C, 4,300 g) on a Beckman Coulter Allegra X-14R Centrifuge with a SX4750A rotor.

Purification of MpIBP

The cellular supernatant was mixed with 16 mL of Ni-NTA (Ni²⁺-nitriloacetate) resin (16 h, 4 °C), loaded into a column, washed with Buffers A through C, and eluted with buffers D and E (Table S2). Fractions were examined using SDS-PAGE, and samples displaying bands for MpIBP (~34kD) were pooled before running through a Thermo-Scientific Protein Biology 50 mL 30kD Pierce Protein Concentrator (2000 g, 4 °C) in Buffer F (tenfold reduction, 3x). The concentrate was loaded onto a DEAE-Sepharose resin column equilibrated with Buffer F, washed with Buffers F through H, and protein was eluted using Buffers I through K (Table S2). Fractions displaying a band for MpIBP via SDS-PAGE were pooled and concentrated, then run on a GE Healthcare AKTApurifier FPLC with a Frac 950 equipped with a HiLoad Superdex 75 PG preparative size exclusion chromatography column. Fractions that displayed a band for MpIBP via SDS-PAGE were again pooled and concentrated.

Concentrate purity was verified using SDS–PAGE (Fig. S1), and absorbance at 280 nm. The final yield was 3 mg of pure *Mp*IBP.

Blue native polyacrylamide gel electrophoresis (BN-PAGE)

Blue-native polyacrylamide gel electrophoresis (BN-PAGE) was performed on MpIBP in varied pH solutions at a concentration of 0.4 mg/ml to ensure visible bands in the gel. BN-PAGE procedures were adapted from Fiala et al. (2011) and Krause and Seelert (2008). Briefly, protein solutions were stained using sample buffer (50 mM bis-tris, 5% w/v Coomassie brilliant blue, 10% glycerol, pH 7). Samples were dry-loaded into a 10% denaturing acrylamide gel (1.75 mm × 10 well; 80 min, 300 mA; outer buffer 1X Tris-glycine native PAGE running buffer, pH 8.3), and run using a voltage of 100 V until the samples entered the separating gel, where the voltage was increased to 150 V. Samples were compared to a 10-250 kDa PageRuler Plus protein ladder (ThermoFisher Scientific) to estimate molecular weight. MpIBP content within the gel was stained using Coomassie SimplyBlue SafeStain (Invitrogen) according to manufacturer specifications.

Size-exclusion chromatography with multiangle light scattering detector (SEC-MALS)

Varied pH solutions were analyzed as controls or loaded with 1 mg/ml *Mp*IBP using size-exclusion chromatography (SEC) equipped with a multiangle light scattering (MALS) detector. SEC was performed on an Agilent 1100 Series LC system and a Tosoh TSKgel G3000SWxl size exclusion column. MALS was performed using a Wyatt miniDAWN Treos II. The mobile phase was 30 mM tris, 150 mM NaCl, and 10 mM CaCl₂ at a flow rate of 0.4 mL/min. 50 μL of each sample were analyzed (50 μg *Mp*IBP/injection). The data were processed using Astra software 7.1.2 and were compared against a bovine serum albumin (BSA) standard to determine size. The data were smoothed using an FFT



algorithm with a 15-point window and plotted using Origin

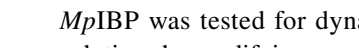
Circular dichroism (CD) spectroscopy

Circular dichroism (CD) spectra were collected on a modular Applied Photophysics Chirascan Plus CD and Fluorescence Spectrometer in the far UV range (190-260 nm) at ambient temperature with 0.5 nm steps and 0.5 s/step at a 0.5 mm path length. MpIBP was loaded at 0.4 mg/ml to ensure adequate detection of the protein. The solutions were tested from 260 nm to a varied minimum wavelength. The final wavelength was altered to be as low as possible per sample before the signal detection limits of the instrument were saturated from the interference of the pH adjusters, namely HCl and NaOH, as they absorb in the peptide bond region (Buck et al. 1954). MpIBP was incubated in solutions for at least 24 h before testing to ensure equilibrium folding states (Song et al. 2007).

Five repeat scans were averaged for each loading of MpIBP in pH solutions and the corresponding baseline for the control pH solution. After removing the control solution baseline, noise was removed from the data in the Chirascan Software using the Savitzky-Golay smoothing filter using five points per window with a polynomial order of two. Protein conformation (% helix, strand, turns, etc.) was measured from the peptide bond region (< 240 nm) (Kelly et al. 2005) using BeStSel software (Misconai et al. 2015) with the exception of the pH 13 sample as the measured data-set did not meet the minimum wavelength range for deconvolution.

Ice recrystallization inhibition (IRI)

Ice recrystallization inhibition of MpIBP was investigated using a splat assay adapted from Knight et al. (1988). Varied pH solutions were tested as controls or with a 0.1 mg/ml loading of MpIBP. Splats were performed in triplicate. A 10 μL droplet of sample was dispensed from 1.7 m through a PVC pipe onto a microscope slide on an aluminum block chilled with dry ice to obtain a single layer of ice crystals. The slide was rapidly transferred to an Otago nanoliter osmometer sample stage annealed at -4 °C for 30 min. The temperature was monitored using a bead-type thermocouple. Ice recrystallization was observed by collecting images immediately after the splat was performed (t_0) to ensure a polycrystalline sample had been obtained, and again at 30 min (t_{30}) to observe IRI activity. Images were taken using an Olympus BX41 microscope with an Olympus PLN 10X objective (NA = 0.25), equipped with an Axiocam 506 color camera on a 1" 1.0×60 N C-mount adapter.



Dynamic ice shaping (DIS)

MpIBP was tested for dynamic ice shaping (DIS) in pH solutions by modifying a protocol established by Bar-Dolev et al. (2012) using an Otago nanoliter osmometer sample stage mounted on an Olympus BX41 microscope with an Olympus LUCPlanFL N 20x /0.45 Ph1 microscope objective (NA = 0.45). MpIBP pH solutions were tested for DIS at a solution concentration of 0.1 mg/ml. Approximately 1 µl sample was loaded into immersion oil in the sample holder for the osmometer, which was carefully placed onto the sample stage atop thermal paste to improve heat transfer. The sample was then frozen rapidly by lowering the temperature to -20 °C. The sample was slowly melted (~ 1 °C/min) until a single ice crystal ($\leq 25 \mu m$) remained. The sample was incubated for 15 min to ensure interaction of MpIBP with the ice surface before the temperature was decreased at 0.01 °C/ min until ice growth occurred. Videos were recorded using Axiocam 506 color camera on a 1" 1.0 × 60 N C-mount adapter. VideoPad Video Editor (NCH Software) was used to isolate still images from video recordings.

Results

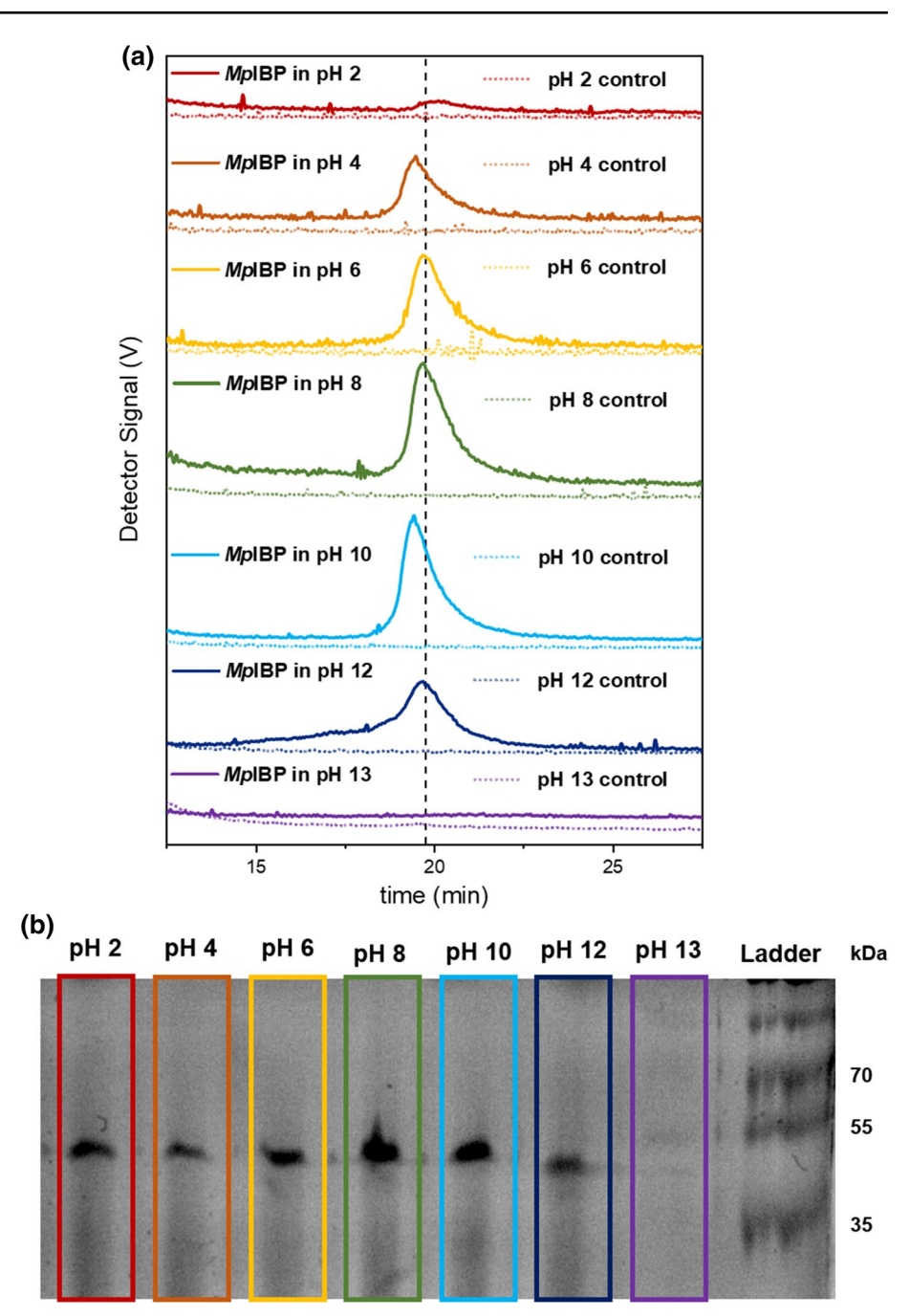
Primary structure of monomeric MpIBP is stable from pH 2 to pH 12

MpIBP was tested for agglomeration and degradation of primary structure in varied pH solutions using SEC-MALS and BN-PAGE, which revealed that the expected protein molecular weight and monomeric state of MpIBP in solution was maintained at pH 4—pH 12, but that hydrolysis and significant degradation occurred at pH 13.

The elution time by SEC-MALS for MpIBP can be related to molecular weight, indicating integrity of the primary structure. A distinct absorbance peak was observed at an elution time of 19.5 min for MpIBP in pH 8 solution, the physiological control pH solution at which we expect MpIBP to be intact (Fig. 1a). MpIBP in solutions at pH 4, 6, and 10 expressed a peak with shape and elution time similar to MpIBP at pH 8 (Fig. 1a). MpIBP in pH 12 solution exhibited peak broadening, with the peak starting at ~ 14.5 min as opposed to 18.5 min. MpIBP in pH 2 solution demonstrated a broad peak at an elution time of 20 min with a reduced intensity compared with MpIBP in pH 8 solution. For MpIBP in pH 2 and pH 12, it is likely that secondary or tertiary structure was disrupted (Feeney et al. 2002) due to changes in the protein's native charge, yielding chromatogram traces with broadened peaks compared with the native protein due to ionic interactions with the column (Barth et al. 1998; Dil 1990). MpIBP in pH 2 may have succumbed to acid mediated hydrolysis (Williams 2003), given



Fig. 1 The stability of *Mp*IBP in pH solutions. a SEC-MALS detector absorbance as a function of elution time for 1 mg/ml *Mp*IBP in solutions with pH 2–13. b BN-PAGE (10% w/v) analysis of 0.4 mg/ml *Mp*IBP stability in solutions with pH 2–pH 13



the reduced intensity and peak broadening observed in the MALS. *Mp*IBP at pH 13 did not evince any peaks, indicating *Mp*IBP did not retain primary structure in this condition.

To verify primary structure integrity, BN-PAGE was performed (Fig. 1b). A clear band for *Mp*IBP at the expected molecular weight was seen in solutions at pH 2 to pH 12, indicating intact primary protein structure. While the predicted molecular weight of *Mp*IBP is 34 kDa, the observed band lies at a higher molecular weight. It is anticipated that the increase in observed molecular weight is likely due to a lack of complete denaturation of the protein, possibly due

to calcium stabilization, and was observed in preceding literature (Garnham et al. 2008). BN-PAGE bands were distinctly absent for *Mp*IBP at pH 13. As there was residual dye in the lanes from running the BN-PAGE, SDS-PAGE was run in addition to verify that there were no smaller protein fragments that may have been obscured by the lane run off (Fig. S2). Only *Mp*IBP at pH 13 exhibited protein bands at lower molecular weights. The lack of a band near 34 kDa and the presence of lower bands for *Mp*IBP at pH 13 corroborates the SEC-MALS result, indicating that *Mp*IBP degraded in pH 13 solution, likely due to hydrolysis



of amino acids (Lawrence and Moore 1951; Radzicka and Wolfenden 1996; Williams 2003).

MpIBP retains secondary structure between pH 6 and pH 10

MpIBP exhibits regularly spaced β-strands that form a β-solenoid. The spacing of the ice-binding residues on the regularly spaced β-strands is currently hypothesized to contribute to its ice-binding activity (Garnham et al. 2008; Guo et al. 2012). Therefore, MpIBP was tested for retention of secondary structure in nonphysiological pH solutions using CD (Fig. 2). The data analysis using BeStSel software parsed secondary structure of MpIBP into eight categories—regular α -helix, distorted α -helix, left β -strand, relaxed β -strand,

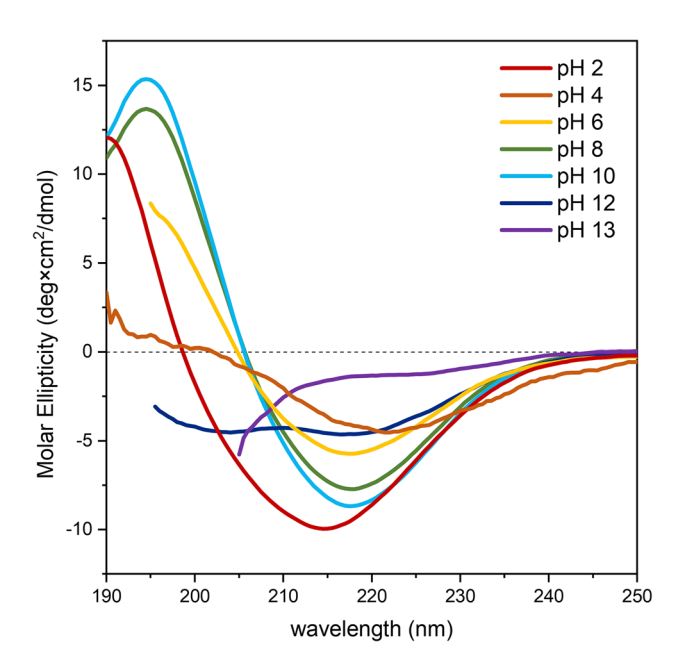


Fig. 2 The far-UV CD spectra of MpIBP in the presence of varied pH solutions (pH 2 (—), pH 4 (—), pH 6 (—), pH 8 (—), pH 10 (—), pH 12 (—), pH 13 (—)). The lowest wavelength was determined by the interference of the pH adjustors and instrument absorption limits

Table 2 Secondary structure of *Mp*IBP under the influence of different pH solutions as determined by BeStSel software

MpIBP structure											
Fold type	pH 2	pH 4	pH 6	pH 8	pH 10	pH 12	*pH 13				
Regular α-helix	35.0%	0.0%	6.9%	20.9%	25.6%	5.8%	_				
Distorted α-helix	11.9%	0.0%	5.4%	1.3%	4.0%	3.1%	_				
Left-twisted antiparallel β-strand	0.0%	1.8%	3.5%	4.7%	3.2%	15.5%	_				
Relaxed antiparallel β-strand	0.0%	0%	0.0%	16.8%	12.7%	0.0%	_				
Right-twisted antiparallel β-strand	14.9%	16.9%	3.1%	3.9%	0.4%	0.0%	_				
Parallel β-strand	11.0%	10.4%	25.2%	26.6%	30.9%	17.1%	_				
Turn	0.0%	39.5%	5.1%	2.1%	1.5%	7.8%	_				
Other (irregular/loop)	27.1%	31.5%	50.7%	23.7%	21.6%	50.8%	_				

^{*}pH 13 was not able to be measured in the minimum range for BeStSel deconvolution

right β-strand, parallel β-strand, turn, and other (disordered) (Table 2).

As expected, ellipticity for MpIBP in the pH 8 control solution exhibited a secondary structure with two distinct peaks: a positive band at 194.5 nm, and a negative band at 218 nm, which matches the spectra previously reported by Garnham et al. (2008) and are indicative of high β -strand content. The CD spectra for MpIBP at pH 10 shows bands in the same locations as pH 8 with a slightly larger magnitude. MpIBP CD spectra in pH 12 solution shows two negative bands at 216.5 and 204 nm. MpIBP CD spectra in pH 13 solution was not able to be measured to achieve a true minimum due to the interference of the pH adjustor with the CD detector. Similar absorbance saturation occurred when measuring the control pH 13 solution due to the pH adjustors. Band shifts can be seen for MpIBP in pH 2 (negative to 215 nm, positive to 190 nm), MpIBP in pH 4 (negative to 221.5 nm, positive to \leq 190 nm), and for MpIBP in pH 6 (negative to 217 nm, positive to \leq 195 nm).

Deconvolution of CD spectra determined that as pH deviated further from pH 8, more changes were imparted to the secondary structure of MpIBP. β -strand structure is important for facilitating ice interactions, and variance the β -strand content in MpIBP secondary structure (left β -strand, relaxed β -strand, right β -strand, parallel β -strand) changed between 13.4% (pH 10) and 48.9% (pH 4) compared with MpIBP in pH 8.

The protein exhibited little change in parallel β -strand content between pH 6 and pH 10, mirroring the structure determined in previous studies (Garnham et al. 2008, 2011; Guo et al. 2012). However, relaxed antiparallel β -strand content was lost entirely at pH 6, whereas it was prevalent at pH 8 and pH 10. At pH \leq 4 or pH \geq 12, the CD spectra indicated that MpIBP secondary structure exhibited larger changes, especially related to β -strand structure. Although MpIBP CD absorption spectra for pH 13 could not be obtained below 205 nm, the spectrum recorded indicates misfolded or unfolded protein (Kelly et al. 2005).



MpIBP exhibits IRI activity between pH 6 and pH 12

IRI assays were implemented to determine the efficacy of MpIBP to prevent ice growth in varied pH environments. As some salts have been shown to effect ice morphology (Wu et al. 2017), control pH solutions without MpIBP were compared to pH solutions with 0.1 mg/ml MpIBP to rule out the influence of salt constituents. Control solutions lacking protein were used in experiments to account for effects due to changes in pH and ionic strength. As expected, all control pH solutions demonstrated ice recrystallization after incubating for 30 min, seen as larger ice grains as compared to ice grains at t₀ (Fig. S3). All control pH solutions exhibited varied ice recrystallization end points (Fig. 3), which is expected due to the addition of pH adjusters (HCl or NaOH) that will affect the hydrogen bonding network of water based on the ion interactions with the bulk, and thus affect the recrystallization process (Wu et al. 2017; Duignan et al. 2014). Control solutions at pH 4, pH 6, pH 10, and pH 12 have larger ice crystals at t₃₀ compared to the control pH 8 solution (Fig. 3). The control pH 2 solution had the same ice recrystallization effect as the control pH 8 solution. Control pH 13 solution exhibits smaller ice crystals at t₃₀ compared to control pH 8 solution, which is expected because an increase in ionic content has been shown to affect the ice recrystallization process and exhibit smaller ice grains (Wu et al. 2017). However, the ionic strength does not inhibit or negate the effect added IBPs (Surís-Valls 2019b).

MpIBP in pH 8 exhibited IRI activity, as evidenced by smaller ice grains than control pH 8 solution at t_{30} (Fig. 3). For pH 6, pH 8, pH 10, and pH 12 solutions, the addition of 0.1 mg/ml MpIBP reduced the growth of ice at t_{30} compared to control pH solutions (Figs. 3, S3). For pH 4 solution, the addition of 0.1 mg/ml MpIBP did not evince IRI activity and ice grain sizes at t₃₀ were the same as control pH 4 solution. For pH 2 and pH 13 solutions, the addition of 0.1 mg/ml MpIBP resulted in larger ice crystals as compared to control solutions. To determine if pH or ionic strength influenced MpIBP activity more, ice grain sizes were estimated and normalized relative to each respective control solution. The mean largest grain size estimates were compared with pH and ionic strength (Fig. S4). It was found that pH had a greater effect on IRI than ionic strength—for example, MpIBP exhibited IRI in pH 12 solution with an ionic strength of 0.078 mol/L, but did not exhibit IRI in pH 2 or pH 4 solutions, each with an ionic strength \leq 0.066 mol/L.

MpIBP exhibits DIS between pH 6 and pH 10

DIS was implemented to determine if *Mp*IBP was adsorbing to the ice crystal surface (Fig. 4). None of the control pH solutions elicited dynamic ice shaping, evidenced by spherical single crystals. DIS by *Mp*IBP was readily seen

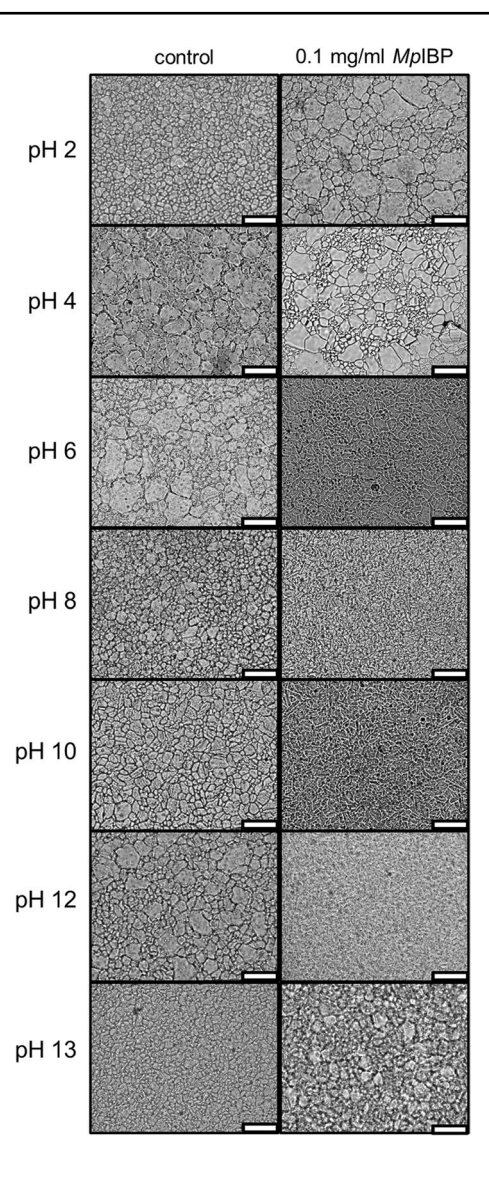


Fig. 3 IRI Micrographs at t_{30} for control pH controls (left) or for 0.1 mg/ml MpIBP in nonphysiological pH solutions (right)

in pH 6, pH 8, and pH 10 solutions as a change to hexagonal ice crystals. At pH \geq 12 or pH \leq 4 MpIBP did not demonstrate any DIS and behaved similarly to control solutions. In physiological solutions, when MpIBP adsorbs to ice crystals it prevents expansion of the crystal in the basal and prism planes, creating a hexagonal ice crystal (Garnham et al. 2008).

Discussion

The results displayed here demonstrate that *Mp*IBP elicits IRI activity between pH 6 and pH 12 and DIS between pH 6 and pH 10. This study investigated *Mp*IBP in various pH environments (pH 2–pH 13). It was found that the primary



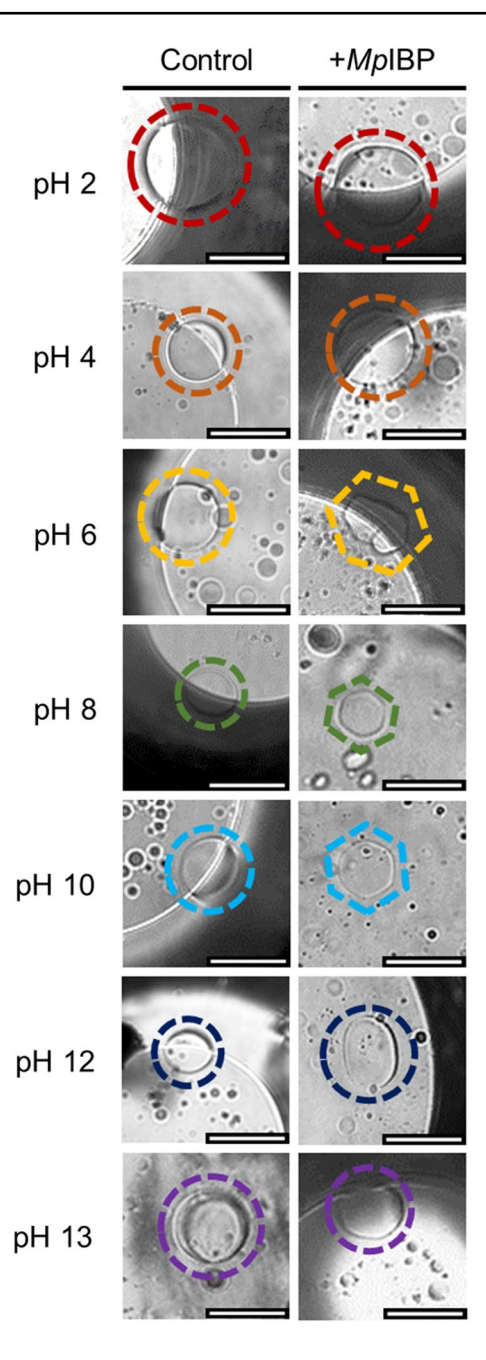
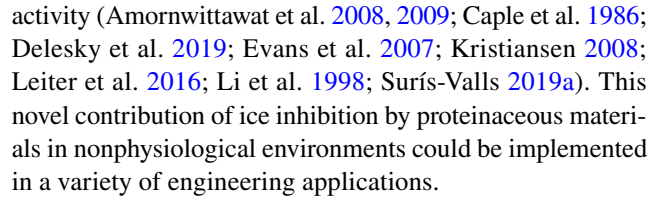


Fig. 4 Dynamic ice shaping for (left) control pH solutions and (right) 0.1 mg/ml MpIBP in pH solutions. Ice crystals outlined with a circle do not demonstrate DIS, and ice crystals outlined with a hexagon demonstrate hexagonal DIS. Bubbles in the images are a result of the immersion oil. Black regions in the images are the sample holder. Scale bar = 50 μ m

structure of monomeric *Mp*IBP is stable from pH 4 to pH 12, and that secondary structure is retained between pH 6 and pH 10. To the authors' knowledge, this is one of only a few studies that looks at the IRI activity of an IBP under the influence of pH adjusted ionic solutions. Most studies investigate IRI activity in neutral ionic solutions or with added polyols, or investigate the change in thermal hysteresis



Based on the singular observable peaks in SEC-MALS and single bands at the expected molecular weight by BN-PAGE, MpIBP does not aggregate or degrade in solutions between pH 4 and pH 12. MpIBP only exhibits degradation in pH 13 solution, made apparent by a lack of elution peak in SEC-MALS and no prominent band at the expected molecular weight by BN-PAGE, as well as smaller molecular weight bands in SDS-PAGE. MpIBP at pH 2 exhibits a broadened peak at the same elution time in SEC-MALS compared to pH 8 but exhibits a band at the expected molecular weight by BN-PAGE, suggesting intact protein with different charge interactions in the SEC-MALS column. The elution peaks for MpIBP in solution with pH 4-pH 12 are singular, and similar in size and elution time as compared to MpIBP in pH 8. Assuming that MpIBP is monomeric at 0.1 mg/ml at pH 8 based on the previous literature (Garnham et al. 2008, 2011), it can be assumed they MpIBP is also monomeric in solutions at pH 4-pH 12. The BN-PAGE showed that the protein was not aggregating due to a lack of upper molecular weight bands, nor was it degrading due to a lack of bands at lower molecular weights, thus the primary structure of the protein is stable.

Properly folded MpIBP creates a calcium-stabilized β-solenoid tertiary structure that would have its ice-binding face exposed to solution, allowing interactions with ice crystals (Fig. 5a). The β-solenoid consists of thirteen tandem repeats with the sequence -xGTGNDxuxuGGxuxGxux-, where x is any amino acid and u is a hydrophobic amino acid (Guo et al. 2012). The current hypothesis for MpIBP ice-binding activity is closely related to its regularly spaced parallel β-strands that promote a 7.4 Å spacing between ice-binding residues (threonine (T) and asparagine (N)) on the same coil of the β -solenoid, as well as 4.6 Å spacing between ice-binding resides on adjacent coils, as can be seen in Fig. 5b (Garnham et al. 2008; Garnham 2011; Guo 2012). Oxygen atoms in the ice crystal lattice repeat at 7.37 Å along the c axis of the primary prism plane as well as repeat at 4.52 Å along the a axis in the primary prism and basal planes, as can be seen in Fig. 5c. The spacing of ice-binding residues along the coils of the MpIBP β -solenoid allow it to match the ice lattice on the primary prism and basal planes of ice, resulting in IRI and hexagonal DIS.

A disruption of protein tertiary structure does not necessarily equate to loss of functionality (Ptitsyn 1987). Small molecule peptide analogs have shown activity, albeit reduced, when compared to their structured counterparts (Surís-Valls 2019b), indicating that if a portion of



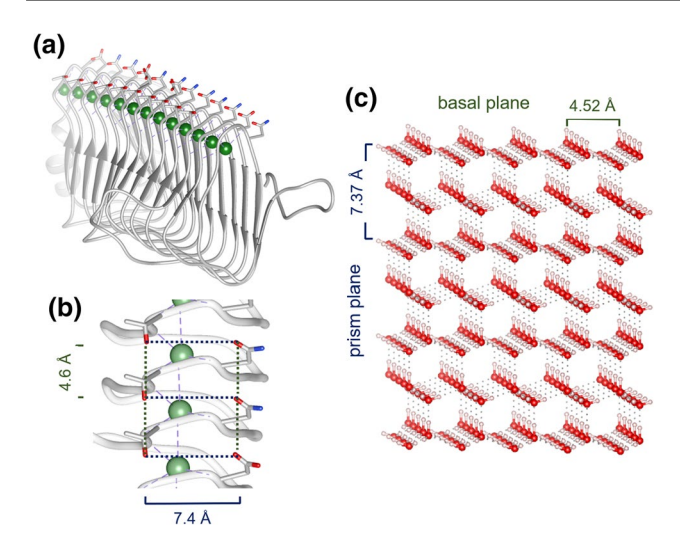


Fig. 5 a The β-solenoid structure of properly folded MpIBP in the presence of Ca²⁺ ions (green spheres). b Spacing of ice-binding residues of properly folded MpIBP. The ice-binding face of MpIBP exhibits ice-binding residues with 7.4 Å spacing on the same coil of the β-solenoid, as well as 4.6 Å spacing between ice-binding resides on adjacent coils. c Schematic of the hexagonal ice crystal lattice. Oxygen atoms in the ice crystal lattice repeat at 7.35 Å along the c axis of the primary prism plane as well as repeat at 4.52 Å along the c axis in the primary prism plane and basal plane. c MpIBP crystal structure was provided by Garnham et al. (2011; PDB 3P4G). c MpIBP molecular graphics performed with UCSF Chimera, developed by the Resource for Biocomputing, Visualization, and Informatics at the University of California, San Francisco, with support from NIH P41-GM103311 (Pettersen et al. 2004). Ice lattice schematic was made using VESTA software (Momma and Isumi 2011)

the protein responsible for ice growth inhibition remains intact, then some activity may be seen. Herein, CD was utilized to hypothesize how changes in secondary structure influenced IRI and DIS activity. CD analysis revealed that MpIBP exhibited relatively well folded structure between pH 8 and pH 10, consisting largely of β-strands, similar to literature precedence (Garnham et al. 2008, 2011; Guo et al. 2012). For MpIBP in pH 10, a change of 23.5% secondary structure, taken as the absolute difference between fold types, is observed although no singular fold type changed by > 5% (Table 2), indicating MpIBP stability at pH 10. Based on the high IRI activity (Fig. 3) and hexagonal DIS for MpIBP in pH 8 and pH 10 solutions, we suggest that the β-helix region hypothesized to interact with ice is intact (Fig. 5a) and can interact with ice crystals to reduce recrystallization (Fig. 3) or alter ice morphology (Fig. 4). Control pH 10 solution exhibited larger grain sizes than control pH 8 solution, demonstrating that for applications in pH 10 environments the crystal expansion would be more detrimental. As the control solution grain size at t_{30} was larger than pH 8 control solution, MpIBPat pH 10 appeared to have the greatest reduction of ice size. Because the grain size at t_{30} for MpIBP at pH 10 was

similar to *Mp*IBP in pH 8 solution, it could be concluded that *Mp*IBP was most effective in pH 10 solution.

MpIBP exhibited promising activity for acidic (pH 6) and basic (pH 12) solutions as a reduction of grain size was observed compared to control solutions, especially considering the final ice grain size for control solutions were larger than control pH 8 solution. MpIBP in pH 6 had a greater reduction of ice size compared to MpIBP in pH 8 at t_{30} . MpIBP in pH 12 demonstrated a reduction of ice crystal size at t₃₀ compared to control pH 12 solution. However, the crystal size for MpIBP in pH 6 and pH 12 at t_{30} was larger than pH 8, indicating decreased IRI activity. The CD spectra for MpIBP in pH 6 demonstrates some folded structure (Fig. 2); however, the BeStSel deconvolution (Table 2) resulted in 50% unfolded structure. MpIBP exhibits a few α -helices and antiparallel β -strands that are not calcium stabilized (Fig. 5a), and it is anticipated that at pH 6 the nonstabilized structures of the protein are beginning to denature while the calcium-stabilized parallel β-strands remain intact. Similar to MpIBP in pH 6, MpIBP in pH 12 solution shows a decrease in secondary structure that is not calcium stabilized while retaining some parallel β -strand structure. As the icebinding residues of MpIBP are regularly spaced between the calcium-stabilized parallel β-strands (Garnham et al. 2011), the retention of the β-strand structure could explain the of IRI activity despite the increase of irregular structure at pH 6. To further probe MpIBP structure under the influence of external stressors such as pH, NMR could be implemented; however, NMR fell outside the scope of this research study.

DIS was only seen in pH 6 and pH 10 solutions where MpIBP showed ≤ 5% change of parallel β-strand structure compared to pH 8, likely because the ice-binding residues still mimicked the distance of oxygen atoms in the ice lattice to facilitate adsorption (Fig. 5). The tertiary structure of MpIBP regularly aligns the ice-binding residues into a 7.4 Å by 4.6 Å motif that facilitates adsorption to hexagonal ice. The 7.4 Å by 4.6 Å motif is structured through the parallel β-strands, and it is anticipated that changes in the β -strand alignment would disrupt the spacing of the residues, reducing the match to the ice crystal lattice. MpIBP in pH 12 retained a similar amount of overall β-strand structure as MpIBP in pH 6. However, MpIBP in pH 12 retained less parallel β-strand and exhibited more twisted β-strand structure. We hypothesize that the increase of twisted β -strand is responsible for the loss of DIS activity as there are no longer enough adjacent coils on the β -solenoid to align the ice-binding residues with an appropriate spacing to match the ice crystal lattice, but the overall retention of general β-strands resulted in IRI activity. As IRI is more reliant on the disruption of water molecules at the ice-water interface between ice grains, retention of any β-strand structure could enable some short-range water ordering to inhibit ice growth. DIS appeared to be more reliant on tertiary structure



than IRI, indicating that there is a minimum amount of native structure required to ensure interaction between the protein and ice (Davies 2014). To better understand how MpIBP can elicit IRI but not DIS in pH 12 solution, it could be beneficial to observe MpIBP in physiological and stressed environments using neutron reflection to determine interactions at the ice—water interface (Xu et al. 2008).

Similar to MpIBP in pH 12, the secondary structure of MpIBP at pH 4 showed an increase in twisted antiparallel β -strands; although MpIBP in pH 4 showed right twisted antiparallel β -strands as opposed to left twisted antiparallel β -strands. However, MpIBP at pH 4 did not evince any IRI activity. It is possible that the difference in the twist direction impacts the difference in IRI activity. Since MpIBP has an isoelectric point of 4.1 (Table S1), MpIBP was expected to exhibit instability in pH 4 solution, which resulted in measurement fluctuations in the CD detector (Xia 2007). It is possible that in pH 4 solution MpIBP is unable to interact with ice due to the net neutral charge of the protein. In the future, to better understand MpIBPs activity around the isoelectric point, solutions with finer gradations of pH could be implemented to glean what might be happening.

Although MpIBP exhibited larger ice crystals compared to control solutions for pH 2 and pH 13, an additional class of proteins, called ice nucleation proteins, can be useful for targeting specific ice crystal sizes in solution (Dolev et al. 2016). The shift of CD spectra to lower wavelengths for MpIBP in pH 2 solution indicates some restructuring with an increase in regular and distorted α -helix structure at the expense of turns, antiparallel β-strands, and parallel β -strands. What β -strand structure that was preserved in MpIBP at pH 2 is again possibly due to calcium stabilization and likely allowed some ice-binding residues to remain exposed to solution. For MpIBP at pH 13, the amount of NaOH necessary to create a pH 13 environment caused absorbance saturation in the CD detector, preventing enough data to be collected for BeStSel deconvolution; however, the spectra that was able to be collected is reminiscent of a typical denatured protein, which is further supported by the lack of elution peak in SEC-MALS and the lack of band at the expected molecular weight by BN-PAGE, indicating protein degradation. It is possible that despite degradation some of the ice-binding residues remained intact on one or more of the sequence repeats (-xGTGNDxuxuGGxuxGxux-). Therefore, it is possible that there were enough ice-binding residues exposed to solution at pH 2 and pH 13 to interact with ice; however, without a regular structure to promote ice growth inhibition, they could facilitate ice nucleation. Ice nucleation proteins typically exhibit a common contiguous octapeptide repeat composed of mainly hydrophilic residues (-AGYGSTLT-) (Kawahara 2017). While MpIPBP does not exhibit more than two adjacent residues from this octapeptide (Fig. S5), there is a -GTG- repeat close to the -GYG- repeat, as well as a high percentage of the hydrophilic residues present in the *Mp*IBP sequence, e.g., 8.2% A, 13.9% G, and 5.7% T (Table S1). To further probe this phenomenon, it would be beneficial to investigate *Mp*IBP in pH 2 and pH 13 as a possible ice nucleator using an ice nucleation assay as described by Congdon et al. (2015). In addition, the sequence of the protein fragments observed at pH 13 could be investigated through mass spectrometry, facilitating understanding of retained amino acid sequences capable of ice nucleation.

To contextualize the importance of investigating ice growth in extreme pH environments, previous research has shown that IRI active materials can decrease freeze—thaw damage in cement due to, in part, to prevent ice crystal expansion (Frazier 2020; Qu 2019). Cementitious materials have a pH of 12–13 due to the presence of Ca(OH)₂ that creates a calcium—silicate—hydrate gel, giving concrete its strength (Ghods et al. 2009) which necessitates pH compatible IRI additives. As Ca²⁺ plays an important role in *Mp*IBP structure, the calcium present in cementitious environments could be advantageous for an *Mp*IBP additive. In addition, since *Mp*IBP prevents ice growth via IRI at pH 12, it could be a beneficial additive to cementitious environments to prevent freeze—thaw damage.

MpIBP exhibits IRI activity in solutions 6 < pH < 12, indicating that MpIBP (and other IBPs) could be effective at mitigating frost-induced damage in applications that necessitate activity in somewhat nonphysiological chemical environments. Although the presence of Na⁺ and Ca²⁺ have been shown to effect ice crystal shape and recrystallization (Wu 2017), no shaping or significant inhibition of ice recrystallization was seen in control solutions pH 6–10, indication that the addition of 0.1 mg/ml MpIBP affected both crystal size (Fig. 3) and shape (Fig. 4). MpIBP is more resistant to the presence of OH⁻ as compared to H₃O⁺, which is substantiated by the isoelectric point of the protein (pI ≈ 4.1). Given that MpIBP is only effective at preventing ice growth in solutions $6 \le pH \le 12$, alternative materials for controlling ice morphology in environments beyond these pH bounds must be considered. To further improve pH stability, synthetic biology approaches could be utilized to engineer a more stable protein that retains activity and mitigates ice growth in environments with a pH < 6 or a pH > 12 (Alegre-Cebollada 2010; Hagan et al. 2010; Kang 2007; Kang and Baker 2009; Zakeri 2015). In addition, synthetic polymer architectures that mimic the ice-binding functionality of IBPs offer a unique avenue for mitigating and controlling ice nucleation and growth, as they may be not only more cost-effective, but also more able to inhibit ice crystal recrystallization in aggressive chemical solutions without relying on tertiary structure to elicit ice interaction activity (Biggs et al. 2017; Congdon et al. 2013, 2015; He et al. 2018; Mitchell et al. 2014, 2015; Stubbs et al. 2019).



Conclusions

This study evaluated the potential of a calcium dependent ice-binding protein (IBP) from Marinomonas primoryensis (MpIBP) to inhibit and control ice crystal nucleation and growth in nonphysiological environments, and changes in activity were found to be a function of protein structure. MpIBP showed the ability to retain its primary and secondary structure in the pH range of 6-10 as indicated by similar CD spectra, a single elution peak in SEC-MALS, and a single band at the expected molecular weight by BN-PAGE. DIS and IRI were observed between pH 6 and pH 10. MpIBP lost parallel β-strand structure at solutions of pH < 6 or pH > 10, as well as the ability to inhibit ice crystal growth and exhibit dynamic ice shaping (DIS). MpIBP at pH 12 was an exception, as it misfolded but still retained IRI activity, though it did not elicit DIS. In the most extreme environments (pH 2 and pH 13), the addition of MpIBP resulted in larger ice crystals after 30 min compared to control solutions. Some applications, such as preventing freeze-thaw damage in cement, require pH resilience for IRI active materials due to a highly alkaline environment (pH 12-13). In conclusion, these results suggest that MpIBP has some applications in nonphysiological environments as frost-prevention materials.

Acknowledgments This research was made possible by the Department of Civil, Environmental, and Architectural Engineering, the College of Engineering and Applied Sciences, and the Living Materials Lab at the University of Colorado Boulder. Thanks to Peter Davies at Queen's University for the gift of the *Marinomonas primoryensus* clones used in this study. A special thanks is given to Dr. Annette Erbse and the Biochemistry Shared Instruments Pool for assistance with CD Spectrometry.

Author contributions Data curation: [EAD]; formal analysis: [EAD], [PET], and [MC]; funding acquisition: [WVSIII]; investigation: [EAD] and [PET]; methodology: [EAD], [PET], [JCC], and [WVSIII]; supervision: [JCC] and [WVSIII]; writing—original draft, [EAD]; writing—review and editing, [PET], [MC], [JCC] and [WVSIII]. All authors have read and agreed to the published version of the manuscript.

Funding This research was funded by the United States (US) National Science Foundation (Award No. CMMI-1727788), the National Science Foundation Graduate Research Fellowship Program, the National Highway's Cooperative Research Program (NCHRP) (Award No. NCHRP-204), and the NIH/CU Molecular Biophysics Training Program (P.E.T.). This work represents the views of the authors and not necessarily those of the sponsors.

Compliance with ethical standards

Conflict of interest The authors declare no conflict of interest. The funders had no role in the design of the study; in the collection, analyses, or interpretation of data; in the writing of the manuscript, or in the decision to publish the results.

References

- Alegre-Cebollada J, Badilla CL, Fernández JM (2010) Isopeptide bonds block the mechanical extension of pili in pathogenic Streptococcus pyogenes. J Biol Chem 285(15):11235–11242
- Amornwittawat N, Wang S, Banatlao J, Chung M, Velasco E, Duman JG, Wen X (2009) Effects of polyhydroxy compounds on beetle antifreeze protein activity. Biochimica et Biophysica Acta (BBA)-Proteins and Proteomics1794(2):341–346.
- Amornwittawat N, Wang S, Duman JG, Wen X (2008) Polycar-boxylates enhance beetle antifreeze protein activity. Biochimica et Biophysica Acta (BBA)-Proteins and Proteomics, 1784(12):1942–1948.
- Bar-Dolev M, Celik Y, Wettlaufer JS, Davies PL, Braslavsky I (2012) New insights into ice growth and melting modifications by antifreeze proteins. J R Soc Interface 9(77):3249–3259
- Bar-Dolev M, Bernheim R, Guo S, Davies PL, Braslavsky I (2016) Putting life on ice: bacteria that bind to frozen water. J R Soc Interface 13(121):20160210
- Barth HG, Boyes BE, Jackson C (1998) Size exclusion chromatography and related separation techniques. Anal Chem 70(12):251–278
- Biggs CI, Bailey TL, Graham B, Stubbs C, Fayter A, Gibson MI (2017) Polymer mimics of biomacromolecular antifreezes. Nat Commun 8(1):1–12
- Buck RP, Singhadeja S, Rogers LB (1954) Ultraviolet absorption spectra of some inorganic ions in aqueous solutions. Anal Chem 26(7):1240–1242
- Caple G, Kerr WL, Burcham TS, Osuga DT, Yeh Y, Feeney RE (1986) Superadditive effects in mixtures of fish antifreeze gly-coproteins and polyalcohols or surfactants. J Colloid Interface Sci 111(2):299–304
- Chao H, DeLuca CI, Davies PL, Sykes BD, Sönnichsen FD (1994) Structure-function relationship in the globular type III antifreeze protein: identification of a cluster of surface residues required for binding to ice. Protein Sci 3(10):1760–1769
- Congdon T, Dean BT, Kasperczak-Wright J, Biggs CI, Notman R, Gibson MI (2015) Probing the biomimetic ice nucleation inhibition activity of poly (vinyl alcohol) and comparison to synthetic and biological polymers. Biomacromol 16(9):2820–2826
- Congdon T, Notman R, Gibson MI (2013) Antifreeze (glyco) protein mimetic behavior of poly (vinyl alcohol): detailed structure ice recrystallization inhibition activity study. Biomacromol 14(5):1578–1586
- Davies PL (2014) Ice-binding proteins: a remarkable diversity of structures for stopping and starting ice growth. Trends Biochem Sci 39(11):548–555
- Davies PL, Hew CL, Fletcher GL (1988) Fish antifreeze proteins: physiology and evolutionary biology. Can J Zool 66(12):2611–2617
- Delesky EA, Frazier SD, Wallat JD, Bannister KL, Heveran CM, Srubar WV (2019) Ice-binding protein from shewanella frigidimarinas inhibits ice crystal growth in highly alkaline solutions. Polymers 11(2):299
- DeVries AL (1988) The role of antifreeze glycopeptides and peptides in the freezing avoidance of Antarctic fishes. Comparative Biochem Physiol Part B 90(3):611–621
- Dill KA (1990) Dominant forces in protein folding. Biochemistry 29(31):7133–7155
- Dolev MB, Braslavsky I, Davies PL (2016) Ice-binding proteins and their function. Ann Rev Biochem 85
- Duignan TT, Parsons DF, Ninham BW (2014) Collins's rule, Hofmeister effects and ionic dispersion interactions. Chem Phys Lett 608:55–59
- Duman JG, Olsen TM (1993) Thermal hysteresis protein activity in bacteria, fungi, and phylogenetically diverse plants. Cryobiology 30(3):322–328



Evans RP, Hobbs RS, Goddard SV, Fletcher GL (2007) The importance of dissolved salts to the in vivo efficacy of antifreeze proteins. Comp Biochem Physiol A 148(3):556–561

- Feeney EP, Guinee TP, Fox PF (2002) Effect of pH and calcium concentration on proteolysis in Mozzarella cheese. J Dairy Sci 85(7):1646–1654
- Fiala GJ, Schamel WW, Blumenthal B (2011) Blue native polyacrylamide gel electrophoresis (BN-PAGE) for analysis of multiprotein complexes from cellular lysates. JoVE (Journal of Visualized Experiments) 48:e2164
- Fletcher GL, King MJ, Kao MH (1987) Low temperature regulation of antifreeze glycopeptide levels in Atlantic cod (Gadus morhua). Can J Zool 65(2):227–233
- Frazier SD, Matar MG, Osio-Norgaard J, Aday AN, Delesky EA, Srubar III, WV (2020) Inhibiting freeze-thaw damage in cement paste and concrete by mimicking nature's antifreeze. Cell Rep Phys Sci 100060.
- Garnham CP, Campbell RL, Davies PL (2011) Anchored clathrate waters bind antifreeze proteins to ice. Proc Natl Acad Sci 108(18):7363–7367
- Garnham CP, Gilbert JA, Hartman CP, Campbell RL, Laybourn-Parry J, Davies PL (2008) A Ca2+-dependent bacterial anti-freeze protein domain has a novel β -helical ice-binding fold. Biochem J 411(1):171–180
- Gauthier SY, Kay CM, Sykes BD, Walker VK, Davies PL (1998) Disulfide bond mapping and structural characterization of spruce budworm antifreeze protein. Eur J Biochem 258(2):445–453
- Ghods P, Isgor OB, McRae G, Miller T (2009) The effect of concrete pore solution composition on the quality of passive oxide films on black steel reinforcement. Cement Concr Compos 31(1):2–11
- Gilbert JA, Hill PJ, Dodd CE, Laybourn-Parry J (2004) Demonstration of antifreeze protein activity in Antarctic lake bacteria. Microbiology 150(1):171–180
- Graether SP, Kuiper MJ, Gagné SM, Walker VK, Jia Z, Sykes BD, Davies PL (2000) β-Helix structure and ice-binding properties of a hyperactive antifreeze protein from an insect. Nature 406(6793):325–328
- Graham LA, Davies PL (2005) Glycine-rich antifreeze proteins from snow fleas. Science 310(5747):461–461
- Griffith M, Ala P, Yang DS, Hon WC, Moffatt BA (1992) Antifreeze protein produced endogenously in winter rye leaves. Plant Physiol 100(2):593–596
- Guo S, Garnham CP, Whitney JC, Graham LA, Davies PL (2012) Re-evaluation of a bacterial antifreeze protein as an adhesin with ice-binding activity. PloS one7(11).
- Hagan RM, Björnsson R, McMahon SA, Schomburg B, Braithwaite V, Bühl M, Schwarz-Linek U (2010) NMR spectroscopic and theoretical analysis of a spontaneously formed Lys-Asp isopeptide bond. Angew Chem Int Ed 49(45):8421–8425
- He Z, Liu K, Wang J (2018) Bioinspired materials for controlling ice nucleation, growth, and recrystallization. Acc Chem Res 51(5):1082–1091
- Hew CL, Slaughter D, Fletcher GL, Joshi SB (1981) Antifreeze glycoproteins in the plasma of Newfoundland Atlantic cod (Gadus morhua). Can J Zool 59(11):2186–2192
- Hoshino T, Kiriaki M, Ohgiya S, Fujiwara M, Kondo H, Nishimiya Y, Tsuda S (2003) Antifreeze proteins from snow mold fungi. Can J Bot 81(12):1175–1181
- Jia Z, DeLuca CI, Chao H, Davies PL (1996) Structural basis for the binding of a globular antifreeze protein to ice. Nature 384(6606):285–288
- Kang HJ, Baker EN (2009) Intramolecular isopeptide bonds give thermodynamic and proteolytic stability to the major pilin protein of Streptococcus pyogenes. J Biol Chem 284(31):20729–20737

- Kang HJ, Coulibaly F, Clow F, Proft T, Baker EN (2007) Stabilizing isopeptide bonds revealed in gram-positive bacterial pilus structure. Science 318(5856):1625–1628
- Kawahara H (2017) Cryoprotectants and ice-binding proteins. In: Psychrophiles: from biodiversity to biotechnology, Springer, Cham, pp 237–257.
- Kelly SM, Jess TJ, Price NC (2005) How to study proteins by circular dichroism. Biochimica et Biophysica Acta (BBA)-Proteins and Proteomics1751(2):119–139.
- Knight CA, Cheng CC, DeVries AL (1991) Adsorption of alpha-helical antifreeze peptides on specific ice crystal surface planes. Biophys J 59(2):409–418
- Knight CA, Hallett J, DeVries AL (1988) Solute effects on ice recrystallization: an assessment technique. Cryobiology 25(1):55–60
- Krause F, Seelert H (2008) Detection and analysis of protein-protein interactions of organellar and prokaryotic proteomes by blue native and colorless native gel electrophoresis. Curr Protocols Protein Sci 54(1):19–18
- Kristiansen E, Zachariassen KE (2005) The mechanism by which fish antifreeze proteins cause thermal hysteresis. Cryobiology 51(3):262–280
- Kristiansen E, Pedersen SA, Zachariassen KE (2008) Salt-induced enhancement of antifreeze protein activity: a salting-out effect. Cryobiology 57(2):122–129
- Lawrence L, Moore WJ (1951) Kinetics of the hydrolysis of simple glycine peptides. J Am Chem Soc 73(8):3973–3977
- Leiter A, Rau S, Winger S, Muhle-Goll C, Luy B, Gaukel V (2016) Influence of heating temperature, pressure and pH on recrystallization inhibition activity of antifreeze protein type III. J Food Eng 187:53–61
- Li N, Andorfer CA, Duman JG (1998) Enhancement of insect antifreeze protein activity by solutes of low molecular mass. J Exp Biol 201(15):2243–2251
- Liang S, Yuan B, Kwon JW, Ahn M, Cui XS, Bang JK, Kim NH (2016) Effect of antifreeze glycoprotein 8 supplementation during vitrification on the developmental competence of bovine oocytes. Theriogenology 86(2):485–494
- Liou YC, Thibault P, Walker VK, Davies PL, Graham LA (1999) A complex family of highly heterogeneous and internally repetitive hyperactive antifreeze proteins from the beetle Tenebrio molitor. Biochemistry 38(35):11415–11424
- Liou YC, Tocilj Å, Davies PL, Jia Z (2000) Mimicry of ice structure by surface hydroxyls and water of a β-helix antifreeze protein. Nature 406(6793):322–324
- Marshall CB, Fletcher GL, Davies PL (2004) Hyperactive antifreeze protein in a fish. Nature 429(6988):153–153
- Micsonai A, Wien F, Kernya L, Lee YH, Goto Y, Réfrégiers M, Kardos J (2015) Accurate secondary structure prediction and fold recognition for circular dichroism spectroscopy. Proc Natl Acad Sci 112(24):E3095–E3103
- Middleton AJ, Vanderbeld B, Bredow M, Tomalty H, Davies PL, Walker VK (2014) Isolation and characterization of ice-binding proteins from higher plants. In: Plant Cold Acclimation, pp 255– 277, Humana Press, New York
- Mitchell DE, Cameron NR, Gibson MI (2015) Rational, yet simple, design and synthesis of an antifreeze-protein inspired polymer for cellular cryopreservation. Chem Commun 51(65):12977–12980
- Mitchell DE, Lilliman M, Spain SG, Gibson MI (2014) Quantitative study on the antifreeze protein mimetic ice growth inhibition properties of poly (ampholytes) derived from vinyl-based polymers. Biomaterials Sci 2(12):1787–1795
- Moffatt B, Ewart V, Eastman A (2006) Cold comfort: plant antifreeze proteins. Physiol Plant 126(1):5–16
- Momma K, Izumi F (2011) VESTA 3 for three-dimensional visualization of crystal, volumetric and morphology data. J Appl Crystallogr 44(6):1272–1276



Pettersen EF, Goddard TD, Huang CC, Couch GS, Greenblatt DM, Meng EC, Ferrin TE (2004) UCSF Chimera—a visualization system for exploratory research and analysis. J Comput Chem 25(13):1605–1612

- Powers TC (1975) Freezing effects in concrete. Special Publication 47:1-12
- Ptitsyn OB (1987) Protein folding: hypotheses and experiments. J Protein Chem 6(4):273–293
- Qu Z, Guo S, Sproncken CC, Surís-Valls R, Yu Q, Voets IK (2019) Enhancing the Freeze-thaw durability of concrete through ice recrystallization inhibition by poly (vinyl alcohol). ACS Omega.
- Radzicka A, Wolfenden R (1996) Rates of uncatalyzed peptide bond hydrolysis in neutral solution and the transition state affinities of proteases. J Am Chem Soc 118(26):6105–6109
- Slaughter D, Fletcher GL, Ananthanarayanan VS, Hew CL (1981) Antifreeze proteins from the sea raven, *Hemitripterus americanus*. Further evidence for diversity among fish polypeptide antifreezes. J Biol Chem 256(4):2022–2026
- Song B, Cho JH, Raleigh DP (2007) Ionic-strength-dependent effects in protein folding: analysis of rate equilibrium free-energy relationships and their interpretation. Biochemistry 46(49):14206–14214
- Stubbs C, Congdon TR, Gibson MI (2019) Photo-polymerisation and study of the ice recrystallisation inhibition of hydrophobically modified poly (vinyl pyrrolidone) co-polymers. Eur Polymer J 110:330–336
- Surís-Valls R, Voets IK (2019a) Peptidic antifreeze materials: prospects and challenges. Int J Mol Sci 20(20):5149
- Surís-Valls R, Voets IK (2019b) The impact of salts on the ice recrystallization inhibition activity of antifreeze (Glyco) proteins. Biomolecules 9(8):347
- Vance TD, Graham LA, Davies PL (2018) An ice-binding and tandem beta-sandwich domain-containing protein in Shewanella frigidimarina is a potential new type of ice adhesin. FEBS J 285(8):1511–1527

- Vance TD, Olijve LL, Campbell RL, Voets IK, Davies PL, Guo S (2014) Ca2+-stabilized adhesin helps an Antarctic bacterium reach out and bind ice. Biosci Rep 34(4).
- Voets IK (2017) From ice-binding proteins to bio-inspired antifreeze materials. Soft Matter 13(28):4808–4823
- Williams AP (2003) Amino Acids Determination In: Encyclopedia of Food Sciences and Nutrition 2nd Ed., Academic, pp 192–197.
- Wu DW, Duman JG, Cheng CHC, Castellino FJ (1991) Purification and characterization of antifreeze proteins from larvae of the beetle Dendroides canadensis. J Comp Physiol B 161(3):271–278
- Wu S, Zhu C, He Z, Xue H, Fan Q, Song Y, Wang J (2017) Ion-specific ice recrystallization provides a facile approach for the fabrication of porous materials. Nat Commun 8:15154
- Xia X (2007) Protein isoelectric point. Bioinformatics and the Cell: Modern Computational Approaches in Genomics, Proteomics and Transcriptomics, 207-21
- Xiao N, Suzuki K, Nishimiya Y, Kondo H, Miura A, Tsuda S, Hoshino T (2010) Comparison of functional properties of two fungal anti-freeze proteins from Antarctomyces psychrotrophicus and Typhula ishikariensis. FEBS J 277(2):394–403
- Xu H, Perumal S, Zhao X, Du N, Liu XY, Jia Z, Lu JR (2008) Interfacial adsorption of antifreeze proteins: a neutron reflection study. Biophys J 94(11):4405–4413
- Zakeri B (2015) synthetic biology: a new tool for the trade. Chem BioChem 16(16):2277–2282

Publisher's Note Springer Nature remains neutral with regard to jurisdictional claims in published maps and institutional affiliations.

